A Data-Driven Building's Seismic Response Estimation Method Using a Deep Convolutional Neural Network

JINKE LI, ZHENG HE, AND XUEFENG ZHAO [ID]
School of Civil Engineering, Dalian University of Technology, Dalian 116024, China
State Key Laboratory of Coastal and Offshore Engineering, Dalian University of Technology, Dalian 116024, China

Corresponding author: Xuefeng Zhao (zhaoxf@dlut.edu.cn)

ABSTRACT As a refined finite element model takes much effort to build and tune to simulate the building structure's response under seismic effects, many rapid estimation methods were proposed to predict the engineering parameters. These methods include simplified structure models, response spectrum, interstory drift spectrum, and machine learning method. This study proposes a method that combines the interstory drift spectrum and a deep learning method to estimate the maximum interstory drift ratio (MIDR). The proposed method includes two approximations. Firstly, use the interstory drift spectrum to estimate the MIDR as a first approximation. Since the differences exist between the interstory drift spectrum and the true responses, the interstory drift spectrum's adjustment is necessary. The second approximation uses a deep convolutional neural network (DCNN) to tune the first approximation to predict the MIDR under a new seismic event. In the training process of the DCNN, 30 reinforced concrete buildings' time history analyses results and 38 interstory drift spectrums were fed into the DCNN. The proposed method is also compared with four artificial neural network models and one support vector machine model to show its advantages. The results indicate that the DCNN could learn the relationship between the interstory drift spectrum and the time history analyses results and make a reasonable prediction of MIDR. Besides, the proposed method is used in MIDR estimation of 30 more detailed finite element models of steel moment-resisting frames. The results indicate that the methodology could give a reasonable estimation of the buildings' MIDR of new seismic events.

INDEX TERMS Convolutional neural network, seismic response prediction, interstory drift spectrum, deep learning, data-driven.

I. INTRODUCTION

In history, seismic disasters have caused countless lives and economic losses to humans. Engineers are working on seismic disaster prevention and reduction in many fields, including structure design, monitoring, vibration control. Because a refined finite element model (FEM) needs time to be built and tuned, researchers proposed different methods to estimate building structures' response under seismic effects rapidly, including simplified models, acceleration spectrum, and machine learning methods.

Many simplified models were proposed to calculate the displacement and force demand for building structures in the design stage. To fulfill this task, researchers proposed different simplified models. Moehle [1] used a response spectrum

analysis method to estimate the reinforced concrete building's maximum inelastic response displacement. Miranda [2] proposed an equivalent continuum structure model consisting of a flexural cantilever beam and a shear cantilever beam to simulate a multistory building's behavior. Miranda's team developed this well-known model in the following works, including lateral stiffness variations' influence on interstory drift demands [3]; assessment of residual displacement ratios [4]; equivalent linear methods to estimate maximum deformation [5]; buildings' behavior under near-fault pulse-like ground motions [6]. Unlike the above methods, Hori's team focuses on the integrated earthquake simulation (IES), including the earthquake propagation in the field. Hori [7] put forward the earthquake computational method to analyze the wave propagation process in the ground, calculating strong ground motions of a target site. Latcharote *et al.* [8] developed this method and utilized the simplified model of

The associate editor coordinating the review of this manuscript and approving it for publication was Nabil Benamar [ID].

four structure types to conduct the seismic risk evaluation in Sendai city, Japan. Sahin *et al.* [9] conducted the IES for Istanbul. In comparison, Lu's team [10]–[12] collect large amounts of experiments and developed a multiple-degree-of-freedom (MDOF) shear model for rapid regional seismic simulation, which could simulate the seismic response of different structure types. Lu *et al.* [10] increased the computing speed of the model using parallel computing conducted on GPU. Xiong *et al.* [11] developed this model by proposing a nonlinear multiple degree-of-freedom flexural-shear model to simulating tall buildings' responses. Xiong *et al.* [12] discussed the parameter determination in the MDOF model and proposed a damage assessment scheme; the MDOF model was validated through three individual tests and one observed seismic damage statistic.

Interstory drift is also a vital engineering parameter in building design and monitoring. Monitoring the interstory drift could evaluate buildings' damage states. Like the response spectrum could give a direct indication of the acceleration demand of earthquake ground motions, the interstory drift spectrum could estimate the interstory drift rapidly based on building periods and damping characteristics [13]. Iwan [13] put forward the interstory drift spectrum for the first time. He simplified the building structure as a continuous linear shear beam and studied the wave propagation in the beam caused by the seismic events. The generated interstory drift spectral could represent the relationship between interstory drifts and fundamental periods or damping ratios. One drawback of this model is that it needs both velocity time histories and displacement time histories of ground motions. However, Kim and Collins [14] pointed out that, in Iwan's model, the residual drift existed at the base in some ground motions when the structure's fundamental period was small. Therefore, researchers developed the interstory drift spectrum using other methods. Chopra and Chintanapakdee [15] used modal analysis to generate the interstory drift spectrum; they suggested the modal participation number should be larger than 5 for a better simulation. Gülkan and Akkar [16] proposed calculating the ground story interstory drift ratio using the ground acceleration, which simplified Iwan's method [13]. Miranda and Akkar [17] also used modal analysis to generate the drift spectrum. They suggested that the first six modes should be considered for a better simulation for buildings with periods longer than 1.2s. However, the model shape depended on the composite beam model [2], which was different from Chopra's model [15]. Shodja and Rofooei [18] proposed a lumped mass beam model to generate an interstory drift spectrum that could consider height-wise stiffness reduction. Neam and Taghikhany [19] used the "Mixed-effects model" to derive a regression model of 851 strong-motion records and study site parameters' effects on the interstory drift spectrum. Guo *et al.* [20] put forward a finite element model for the composite beam [2] and a self-similar interstory drift spectrum; the self-similar interstory drift spectrum was evaluated under the idealized pulses and near-fault ground motions.

With the development of computer hardware like CPU, GPU, and storage, Machine Learning (ML) and Deep Learning (DL) make breakthroughs in recent years. As ML algorithms perform well in processing large amounts of data, their application in seismic response prediction is spontaneous. Artificial Neural Network (ANN) is an ML algorithm to obtain the relationship between input and output through a multilayer perceptron. Lautour and Omenzetter [21] used an ANN model to predict seismic-induced structural damage. In their work, the ANN model's input parameters include 13 structure parameters and six seismic parameters. Kalman Šipoš *et al.* [22] used ANN to predict framed-masonry structural elements' seismic behavior and conduct a sensitivity analysis of the essential factors. To distinguish the different seismic events, Morfidis and Kostinakis [23] used 14 seismic parameters representing ground motions' properties; they evaluated the weights of 14 seismic parameters in the network. They also estimate the maximum interstory drift ratio (MIDR) of new seismic events using two ANN models [24], with 14 seismic parameters used in the input. Mangalathu *et al.* [25] used an ANN model to generate bridge-specific fragility curves.

However, the above three methods have some disadvantages. Although both the simplified model and the interstory drift spectrum could give a rapid estimation of the MIDR, differences between the true response and the estimation may exist due to the modeling error or building information absence like stiffness, damping ratio, material behavior. Tuning these parameters is time-consuming work that will take many human efforts. The ML method usually has a good prediction performance when the features have been used in the training set. When the features are quite different from those in the training set, the prediction results always perform poorly. For example, the ML method has a relatively bad performance in predicting structure response under new seismic events, which have not been used in the training set.

Recently, the DL is much developed, especially in image recognition and data process. The Convolutional Neural Network (CNN) has some advantages: sparse interactions, parameter sharing, and equivariant representations [26]. Based on the data characteristics, CNN could handle different kinds of works. Two-dimension (2D) CNN often handles image-related problems such as image identification, image reconstruction. For example, Li *et al.* [27] propose a convolutional encoder-decoder network to detect crack from concrete images. Zhang *et al.* [28] put forward a multi-point displacement monitoring method based on a full convolutional neural network. Although the acceleration signal or other monitoring signals are always one-dimension (1D) signals, some researchers construct some ingenious data structures to import into 2D CNN. Modarres *et al.* [29] used the modal strain energy to construct the honeycomb panels' damage index. The damage index pictures were imported into a CNN to classify the damage conditions into three types. Cofre-Martel *et al.* [30] collected ten different transmissibility functions measured on a structural beam to generate
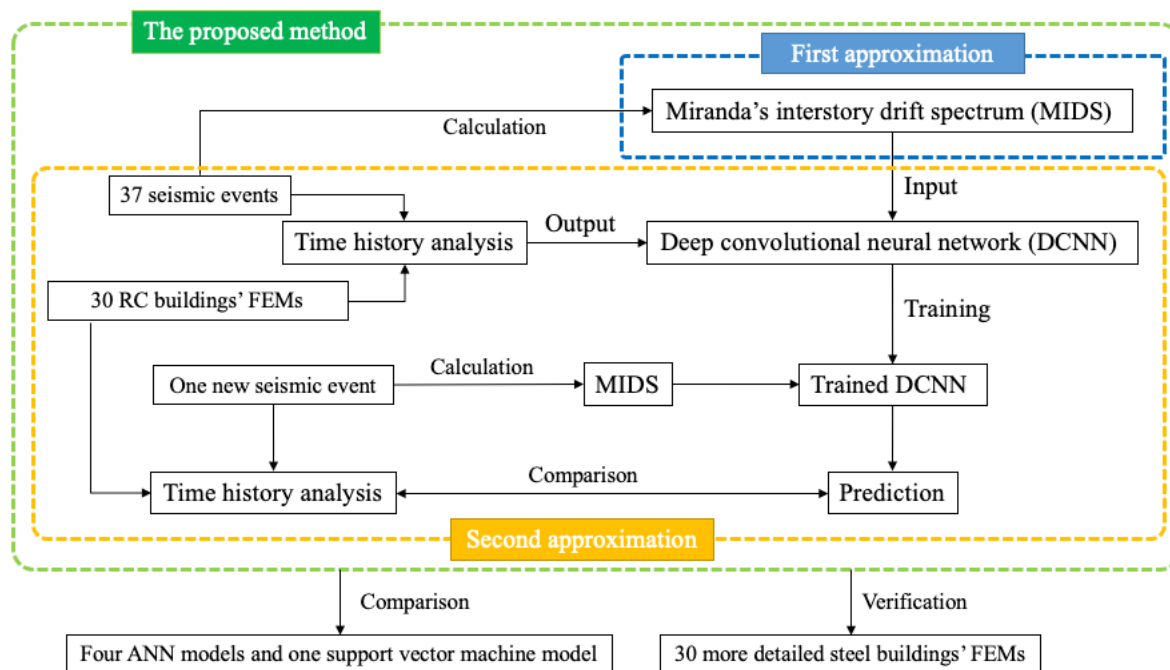
images with 10*96 pixels. After feeding the images into the CNN, the network was trained and verified through two different experiments. Yu *et al.* [31] adopted frequency domain signals of several sensors to compose 2D images, which were import into a CNN for damage identification. Dong *et al.* [32] construct a CNN to distinguish two seismic waveforms of microseismic events and blast.

In contrast, 1D CNN could handle time-variant data like monitoring data, cardiogram cardiograph electrocardiogram. Fan *et al.* [33] used CNN to recover the lost vibration data in structural health monitoring. A deep CNN network named SHMnet proposed by Zhang *et al.* [34] could process the vibration data to detect the bolted connection damage. Guo *et al.* [35] utilized multiple convolutional layers to construct a 1D CNN. It is combined with multiple residual learning modules; the network could extract the damaged features from the noisy and incomplete model shapes.

This study combines the interstory drift spectrum and a DL method to estimate the buildings' MIDR to overcome traditional rapid estimation methods' drawbacks. Two approximations are made to predict the MIDR. First, use Miranda's interstory drift spectrum (MIDS) to give a first approximation of the MIDR. Second, use the DL method to tune the MIDS and give a second approximation of the MIDR so that the prediction will be more precise. The flow chart of the proposed is shown in Figure 1.

This study proposes a data-driven method based on DCNN to estimate the buildings' MIDR under new seismic events. First, the interstory drift spectrum of 38 seismic events was calculated. Simultaneously, time history analyses (THA) of 30 reinforced concrete (RC) buildings were conducted

under 38 seismic events. A DCNN model was designed according to the data structure of the interstory drift spectrum. Meanwhile, the MIDS and the THA results were imported into the DCNN as the input and output. Compare the DCNN's predictions with the THA results to verify the DCNN's feasibility. Besides, the proposed method was compared with four ANN models and one support vector machine model to show its robustness. Finally, the proposed method was verified through 30 more detailed steel moment-resisting buildings' FEMs.

II. PROPOSED APPROACH

This section will introduce some conceptions and some model details, including a basic conception of the interstory drift spectrum, two kinds of time history analyses, two DCNN models, four ANN models, and one support vector machine model. At last, the framework of the proposed method is summarized. In this study, there are two assumptions: 1. The materials of FEMs are elastic. 2. The time history analyses only consider one direction of the buildings' seismic response.

A. INTERSTORY DRIFT SPECTRUM

MIDS is used in this study, and it is based on Miranda's composite beam model [2], [3], [17]. Using interstory drift spectrum, buildings' MIDR could be obtained based on fundamental period. Roughly speaking, the composite beam model comprises a flexural cantilever beam and a shear cantilever beam. As shown in Figure 2, the two beams are connected by some axially rigid members so that the horizontal force could transmit, with the same lateral deformation at
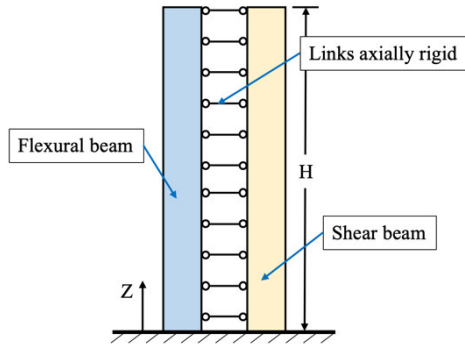
FIGURE 2. A scheme of the composite beam model.

FIGURE 3. An explanation of MIDR.

a certain height. The corresponding descriptions had been presented in the previous studies [2], [3], [17], [36], but they are also depicted for a better understanding. The following equations do not consider the height-wise stiffness variation.

The paper [36] gives the representation of the model shape $\phi_i(x)$, and the derivative of the mode shapes $\phi_i'(x)$ of the composite beam model (x is a non-dimensional height as x = z/H, H is the building height.):

$$\phi_i(x) = \sin(\gamma_i x) - \frac{\gamma_i}{\beta_i} \sinh(x\beta_i) - \eta_i \cos(\gamma_i x) + \eta_i \cosh(\beta_i x) \qquad (1)$$

$$\phi_i'(x) = \gamma_i \cos(\gamma_i x) - \gamma_i \cosh(x\beta_i) + \eta_i \gamma_i \sin(\gamma_i x) + \eta_i \beta_i \sinh(\beta_i x) \qquad (2)$$

where two non-dimensional parameters are defined as:

$$\beta_i = \sqrt{\alpha^2 + \gamma_i^2} \qquad (3)$$

$$\eta_i = \frac{\gamma_i^2 \sin(\gamma_i) + \gamma_i \beta_i \sinh(\beta_i)}{\gamma_i^2 \cos(\gamma_i) + \beta_i^2 \cosh(\beta_i)} \qquad (4)$$

Moreover, α is defined as a ratio of shear rigidity to flexural rigidity:

$$\alpha = H\sqrt{\frac{GA}{EI}} \qquad (5)$$

where GA is the shear beam's shear rigidity, EI is the flexural beam's flexural rigidity. In (3), γ_i is the eigenvalue of i th mode of (6):

$$2 + \left(2 + \frac{\alpha^4}{\gamma_i^2 \beta_i^2}\right) \cos(\gamma_i) \cosh(\beta_i) + \left(\frac{\alpha^2}{\gamma_i \beta_i}\right) \sin(\gamma_i) \sinh(\beta_i) = 0 \qquad (6)$$

Besides, the modal participation factor Γ_i is expressed as:

$$\Gamma_i = \frac{\int_0^1 \phi_i(x)\, dx}{\int_0^1 \phi_i^2(x)\, dx} \qquad (7)$$

The interstory drift ratio (IDR) at height x and time t can be approximated as:

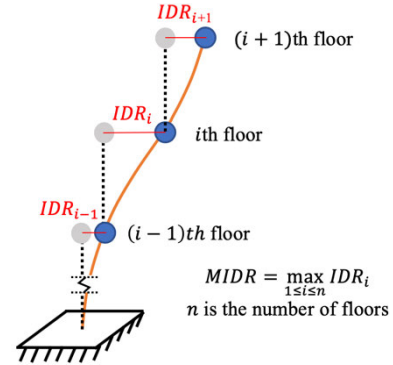$$IDR(x, t) \approx \frac{1}{H} \sum_{i=1}^m \Gamma_i \phi_i'(x) D_i(t) \qquad (8)$$

where m is the model number considered, $D_i(t)$ is the relative displacement response of a single degree of freedom system subjected to a ground acceleration $\ddot{u}_g(t)$, with a period T_i, modal damping ratio ξ_i of i th mode. The single degree of freedom system' damping ratio of each mode is 0.05 in this study. The interstory drift spectrum is defined as the MIDR along the height x and the vibration period t.

$$MIDR = IDR_{max} = \max_{\forall x, t} IDR(x, t) \qquad (9)$$

In this study, the first six modes were considered in the calculation because paper [17] concluded that the six modes of vibration are enough to obtain MIDR demands for all fundamental periods.

From (1) to (9), with a certain fundamental period, the MIDS depends on the stiffness ratio α and the damping ratio ξ_i. The height-wise stiffness variation is also an essential factor because the original building usually has stiffness variation, which is not easy to be simulated in the theoretical derivation. Researchers have to assume the stiffness variation shape like linear, parabolic to consider its influence on buildings' dynamic behavior [3], [18], [37], [38].

B. TIME-HISTORY ANALYSIS (THA)
1) THE MULTISTORY CONCENTRATED-MASS SHEAR MODEL
This study first adopts the multistory concentrated-mass shear (MCS) model proposed by Lu [10]–[12] to conduct THA under seismic effects. In an MCS model, each floor of a building is simplified as a concentrated mass. Once the building details like structure type, floor number, floor area have been identified, the MCS model could generate an OpenSees [39] script. Finally, engineering parameters such as MIDR, roof displacement, acceleration time-history of each floor could be calculated by the FEM.

MIDR, which is a common engineering parameter, can be illustrated in Figure 3. Due to the simplicity of the MCS model, the 30 RC building models could be generated quickly, and thus it is used for the preliminary verification. The RC building, corresponding to structure type C1 (concrete moment frame) in HAZUS [40], is used first. Because this study only considers the elastic demand, each floor's bilinear hysteretic material model is not used. Besides,
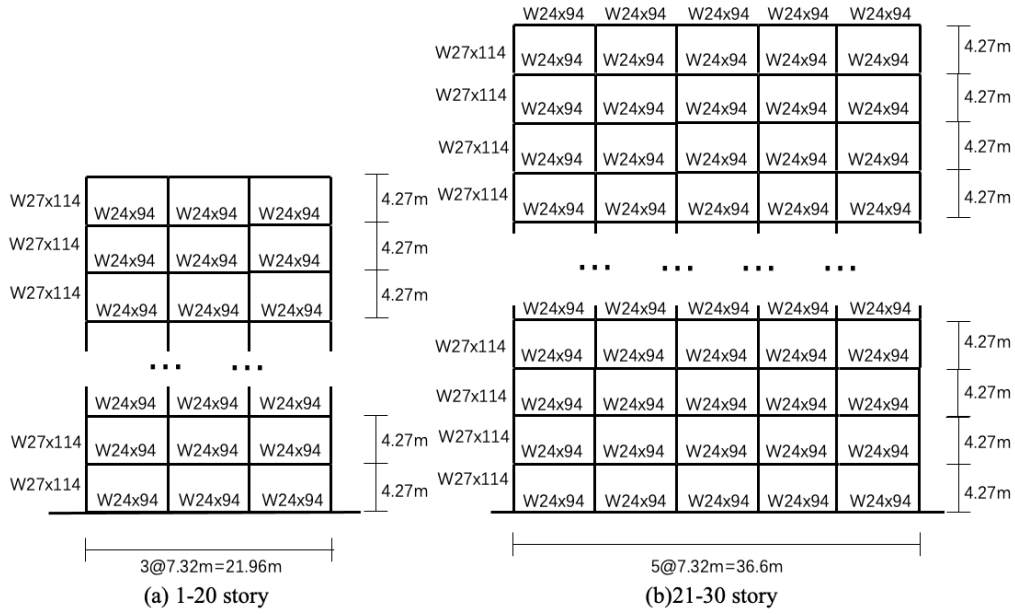
FIGURE 4. The SMRF buildings' FEMs.

TABLE 1. The building attributes in the MCS models.

Structure type	Floor mass	Floor number
C1 (concrete moment frame)	10^6kg	1-30

the lumped mass of each floor is the same as 10^6kg. Some empirical formulas have already regressed the relation between fundamental periods and building height, which is monotonically increasing. Thus, the only variable is the floor number varied from 1 to 30 resulting in 30 different fundamental periods. There are 30 building FEMs in the simulation (TABLE 1). Gathering the calculation results of 30 buildings could identify a discrete interstory drift spectrum (DIDS).

The external load of 30 FEMs is the seismic effects on the foundation node. There are 38 seismic waves on the soil site downloaded from PEER [41]. The information and parameters of all seismic events are listed in TABLE 2. Each wave has already been scaled to the one-tenth of its origin peak ground acceleration to avoid the inelastic response. Besides, only the fault normal (FN) component is considered in the THA.

2) THE STEEL MOMENT-RESISTING FRAME FEM

Except for the MCS models, use 30 more detailed steel moment-resisting frame (SMRF) FEMs (Figure 4) to verify the proposed method. These models conducted the THA, resulting in MIDR as an input in the DCNN model. These SMRF buildings have a uniform lateral stiffness along with the building height.

The details of the material properties are listed in TABLE 3. 30 SMRF buildings' differences are mainly the story height
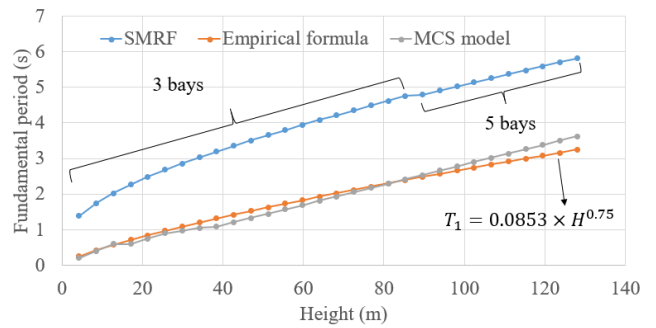

FIGURE 5. Fundamental periods with respect to building heights.

(1-30 story). The higher the SMRF, the bigger the fundamental period is.

The fundamental periods of the two models are shown in Figure 5. The fundamental periods of the MCS models are close to the empirical formula [42]:

$$T_1 = 0.0853H^{0.75} \tag{10}$$

where H is building height in meters, T_1 is the fundamental period. In contrast, the periods of the SMRF model are greater than that of the MCS model.

The SMRF models use the Rayleigh damping ratio. The first mode and third mode's damping ratios are assumed as 4%. 30 SMRF buildings will be subjected to the 38 ground motions in Table 2 without scaling. The calculations were conducted using OpenSees software. The above SMRF models are based on one OpenSees example [43].

C. DEEP CONVOLUTIONAL NEURAL NETWORK

The basic concepts of DCNN could be found in the references [29], [44], including the convolution layer,

TABLE 2. Details of the ground motion records.

Record number	Earthquake Name	Year	Station	Magnitude	Direction
1	Mammoth Lakes-01	1980	Long Valley Dam (Upr L Abut)	6.06	FN
2	Chi-Chi, Taiwan	1999	CHY036	7.62	FN
3	Imperial Valley-06	1979	Delta	6.53	FN
4	Kocaeli, Turkey	1999	Yarimca	7.51	FN
5	Imperial Valley-06	1979	Calipatria Fire Station	6.53	FN
6	Chi-Chi, Taiwan	1999	CHY034	7.62	FN
7	Chi-Chi, Taiwan	1999	NST	7.62	FN
8	Kocaeli, Turkey	1999	Duzce	7.51	FN
9	Trinidad	1980	Rio Dell Overpass, E Ground	7.2	FN
10	Spitak, Armenia	1988	Gukasian	6.77	FN
11	Loma Prieta	1989	Gilroy Array #4	6.93	FN
12	Chi-Chi, Taiwan	1999	TCU060	7.62	FN
13	Victoria, Mexico	1980	Chihuahua	6.33	FN
14	Loma Prieta	1989	Fremont - Emerson Court	6.93	FN
15	Chalfant Valley-02	1986	Zack Brothers Ranch	6.19	FN
16	Chi-Chi, Taiwan	1999	TCU118	7.62	FN
17	Denali, Alaska	2002	TAPS Pump Station #10	7.9	FN
18	Imperial Valley-06	1979	El Centro Array #4	6.53	FN
19	Big Bear-01	1992	San Bernardino - E & Hospitality	6.46	FN
20	Northridge-01	1994	Sylmar - Converter Sta	6.69	FN
21	San Fernando	1971	LA - Hollywood Stor FF	6.61	FN
22	N. Palm Springs	1986	Morongo Valley	6.06	FN
23	Loma Prieta	1989	Hollister - South & Pine	6.93	FN
24	Chi-Chi, Taiwan	1999	TCU055	7.62	FN
25	Chi-Chi, Taiwan	1999	CHY025	7.62	FN
26	Imperial Valley-06	1979	Brawley Airport	6.53	FN
27	Chi-Chi, Taiwan	1999	CHY088	7.62	FN
28	Duzce, Turkey	1999	Duzce	7.14	FN
29	Chi-Chi, Taiwan	1999	TCU061	7.62	FN
30	Loma Prieta	1989	Saratoga - Aloha Ave	6.93	FN
31	Imperial Valley-02	1940	El Centro Array #9	6.95	FN
32	Chi-Chi, Taiwan-03	1999	TCU123	6.2	FN
33	Northridge-01	1994	Jensen Filter Plant	6.69	FN
34	Chi-Chi, Taiwan-03	1999	CHY104	6.2	FN
35	Loma Prieta	1989	Salinas - John & Work	6.93	FN
36	Loma Prieta	1989	Coyote Lake Dam (Downst)	6.93	FN
37	Chi-Chi, Taiwan	1999	CHY008	7.62	FN
38	Chi-Chi, Taiwan-06	1999	TCU141	6.3	FN

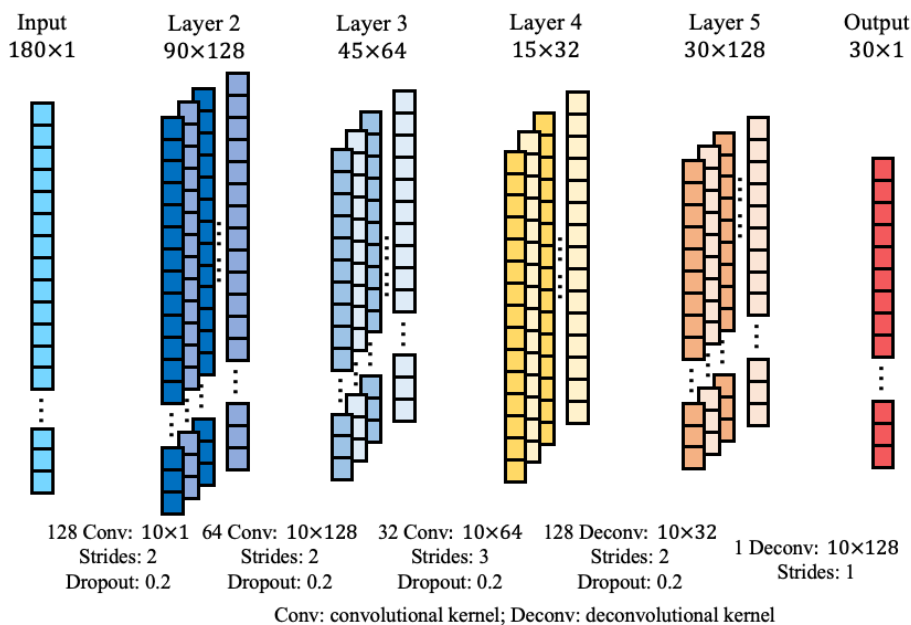| Story	Bay	Material model	Elastic Modulus	Poisson's ratio	Weight (KN/m)		
					Slab	Beam	Column
1-20	3	Elastic	199.96Gpa	0.3	26.25	1.37	1.66
21-30	5						

FIGURE 6. The DCNN1's configuration.

convolutional kernel, activation function, training, drop out. These basic conceptions are not described in this article to avoid repetition.

The networks used below are inspired by the autoencoder. The simplest autoencoder is a multilayer network with an attempt to copy its input to its output. Thus, the middle of the hidden layer or the bottleneck layer has the least neurons through a multilayer architecture. Attribute to this structure, low dimension features could be drawn out of raw data. Autoencoder is competent in signal reconstruction, dimensionality reduction, and feature learning [26]. Autoencoder has many engineering applications like data anomaly automatically [45], wave pattern recognition [46]. When autoencoder is combined with CNN, the first half needs convolution operations to decrease the dimension. At the same time, the left half need deconvolution operations to increase the dimension. The problem in this study also involves finding the relationship between the input (MIDS) and the output (DIDS) and reconstructing the input. Although the input and the output dimension are not the same, convolution operations and deconvolution operations are also kept in the architecture. Additionally, two networks that only have convolution operations (denoted as C1 and C2) are used for comparison.

The framework of the DCNN in this study could be described as follows. There are two DCNNs denoted as DCNN1 and DCNN2. DCNN1 processes the MCS models' results; DCNN2 processes the SMRF models' data. The main difference between the two models is the length of the input data. Figure 5 shows that, in DCNN1, the 30 MCS models' fundamental periods vary from 0.2s to 3.62s. The MIDS's fundamental periods' selection varies from 0.2s to 3.78s with an interval of 0.02s (180 data) to include period 3.62s in the dataset. In contrast, in DCNN2, the 30 SMRF models' fundamental periods range from 1.38s to 5.82s. Similarly, the corresponding MIDS's fundamental periods start from 0.02s, end at 5.94s (288 data).

The architecture of DCNN1 is illustrated in Figure 6. The parameters of DCNN1 are determined through experience and trial and error. DCNN1 has six layers in total; the shape of the input layer and the output layer are 180×1 and 30×1, respectively. In the middle of the network, the data character varies with the convolutional kernel size. After the input layer, 128 convolutional kernels, with a size of 10×1 (1 is the kernel depth) and a stride of 2, were used to conduct convolution calculation with the input layer's data. Each kernel generates one channel of the feature map in the next sub-sampling layer, and the depth of the convolutional layer equals the number of the kernel [31]. Between the input layer and layer 2, there is a dropout layer to avoid overfitting. The dropout obeys a Bernoulli distribution with a probability of 0.2. Subsequently,
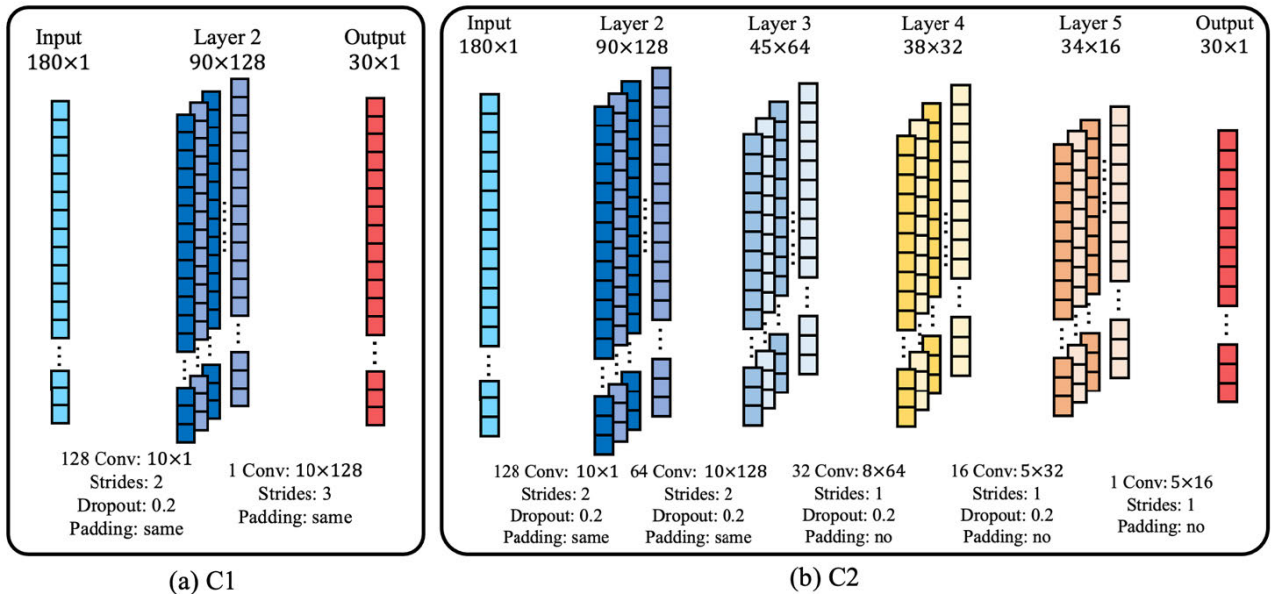
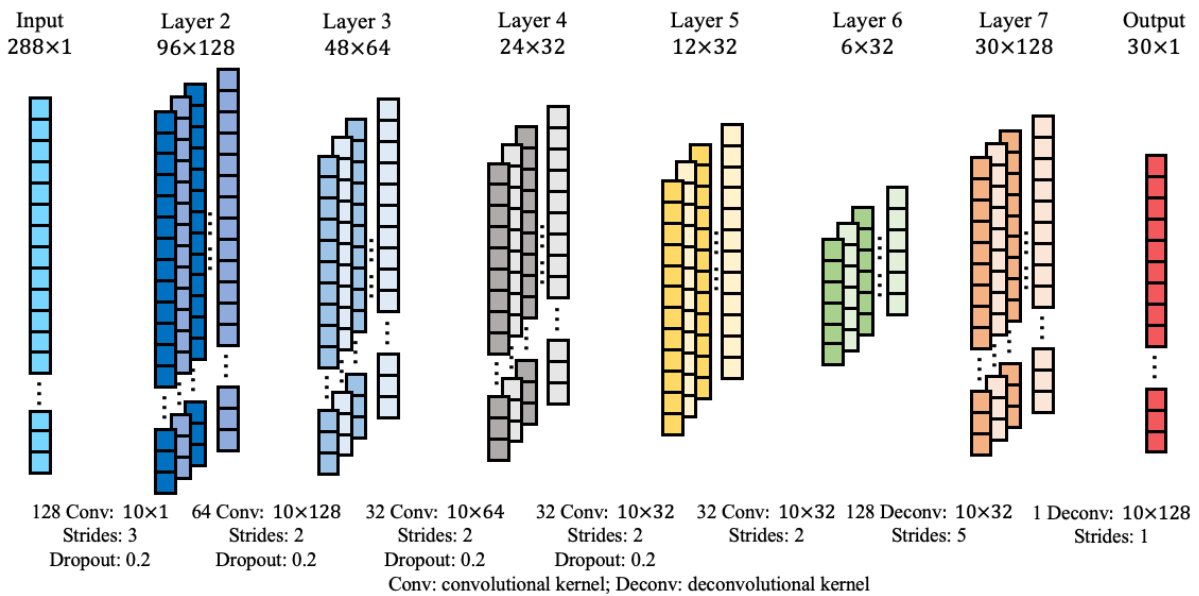**FIGURE 7.** Two networks only have convolution operations.

FIGURE 8. The DCNN2's configuration.

64 convolutional kernels with size 10 × 128 (128 is the kernel depth) and stride of 3 were used to do convolution calculation with layer 2. The feature maps have structures of 45 × 64 in layer 3. Layer 4 is the bottleneck of the DCNN due to its shortest data length (15). To sum up, the first half contains convolutional layers. The data size decreases from 180 to 15 in the down-sampling process, but the feature maps' number increases along with the convolutional kernels' number.

The second half uses deconvolutional layers (or transposed convolutional layers) to increase the data length. Deconvolutional layers could convert a coarse input tensor into a dense output tensor. The details of the deconvolution calculation could be found in the paper [44], section 3.3. The deconvolution calculations in layer 4 and layer 5 have strides 2 and 1, respectively, which result in the increase of the data size. In layer 5, use only one deconvolutional kernel with size ten and depth 128 so that the output layer will have a data size of 30 × 1. The details of the rest could be seen in Figure 6.

Additionally, two networks only have convolution operations as comparisons of the DCNN1, as shown in Figure 7. C1 has the simplest architecture with only one middle layer. By contrast, C2 has more layers with descending dimensions. The gradually descending dimensions are fulfilled through different strides and zero-padding strategies.

Additionally, the DCNN2's configuration is shown in Figure 8. The configuration is similar to the DCNN1 except for a different input data size (288) and a deeper network (eight layers). Accordingly, the convolutional kernel size and the feature map size are different in each layer. There is one thing to be noted, in the convolution and deconvolution operation of the two networks (DCNN1 and DCNN2), the zero-padding setting is "same," which means the input and the output have the same dimension in convolution operation when the stride is 1.

Before the training process, the raw data were regularized through linear scaling to prevent overfitting, as shown in (11):

$$x_{scaled} = \frac{x - x_{min}}{x_{max} - x_{min}} \qquad (11)$$

where x is the MIDS value, x_{min} and x_{max} are the minimum and maximum value, x_{scaled} is the scaled value. After regularization, the MIDS will be scaled to the interval [0, 1]. Besides, the loss function of the network is mean square error (MSE) [47]. The optimization algorithm used is adaptive moment estimation (ADAM) [29] aiming to find the direction where the loss function could be decreased, and the kernels could be tuned accordingly.

Because there are only 38 seismic waves in the dataset, 38-fold cross-validation is used in training. In other words, 37 waves were used as the training set; the left one was used as the validation set. Therefore, the training was conducted 38 times to test performance. During the training process, early stopping was used, with patience set 100. It means that the training process stops when the validation loss does not decrease for 100 epochs. Early stopping could prevent the overfitting effectively. Too many epochs in the training may result in over fitting if the stop epoch is just set a large number. The network was conducted in software PyCharm using Python library Keras [48] to build, train, and evaluate the model. Each model spends about 3min in training, conducted on a computer with intel®Core™i7-4790 CPU, 32G RAM.

D. ARTIFICIAL NEURAL NETWORK MODEL

In this study, the proposed method is compared with four ANN models. ANN could be recognized as a multilayer perceptron [49]. The output of each perceptron could be identified through equation (12):

$$y_k = f\left(\sum_i w_i x_i + b_k\right) \qquad (12)$$

where x_i is the input value, w_i is the weight, b_k is bias, f is the activation function. Then, y_k could be used as the input of the perceptron in the next layer. ANN has been successfully used in civil engineering and seismic response estimation [22], [23], [50], [51]. To estimate the building's seismic response, the four ANN models acquire the characteristics of the models proposed before [21], [23], [24]. In the models before, the features used in ANN involve two parts. One part includes structure parameters, which aim to learn the structural differences. The other part includes seismic parameters,

TABLE 4. 38 Ground motions' seismic parameters.

Parameter	Abbreviation
Peak Ground Acceleration	PGA
Peak Ground Velocity	PGV
Peak Ground Displacement	PGD
Vmax / Amax	PGV/PGA
Arias Intensity	Ia
Specific Energy Density	SED
Cumulative Absolute Velocity	CAV
Acceleration Spectrum Intensity	ASI
Housner Intensity	HI
Effective Design Acceleration	EDA
Predominant Period	PP
Time of Uniform Duration	TUD
Time of Bracketed Duration	TBD
Time of Significant Duration	TSD

which attempts to consider ground motion's characteristics. Thus, the ANN models used here consider both the structure parameters and the seismic parameters. There are 14 seismic parameters to discriminate each seismic event. These seismic parameters were obtained using software SeismoSignal [52] as shown in TABLE 4.

The 30 MCS models only have differences in story number, which can also be reflected by the fundamental period. Consequently, the first two ANN models (denoted as M1 and M2) choose the fundamental period as a structure parameter. M2 has one more hidden layer than M1, as shown in Figure 9. The added one hidden layer aims to add the network's depth, improving the ability to find a nonlinear relationship. However, ANN will not obtain the best performance by simply adding the hidden layer number according to the experiences in designing an ANN model [45]. In the middle of the network, there are 20 neurons in each hidden layer. The output layer has only one neuron (MIDR) because the M1 and M2 aim to predict the buildings' MIDR. The nonlinear relationship between the input and the output is realized through a multilayer perceptron.

In contrast to M1 and M2, the other two ANN models (denoted as M3 and M4, as shown in Figure 10) have one more input neuron named MIDS of a certain fundamental period (MIDSFP). MIDSFP could give a first estimation of the MIDR using the interstory drift spectrum. Based on one MIDSFP value, one structural feature, and 14 seismic features, the M3 and the M4 are expected to estimate the MIDR better.

E. SUPPORT VECTOR MACHINE MODEL

Support vector machine (SVM) is also used in this study for comparison. SVM is a widely used supervised learning algorithm, which could be used in classification and regression.
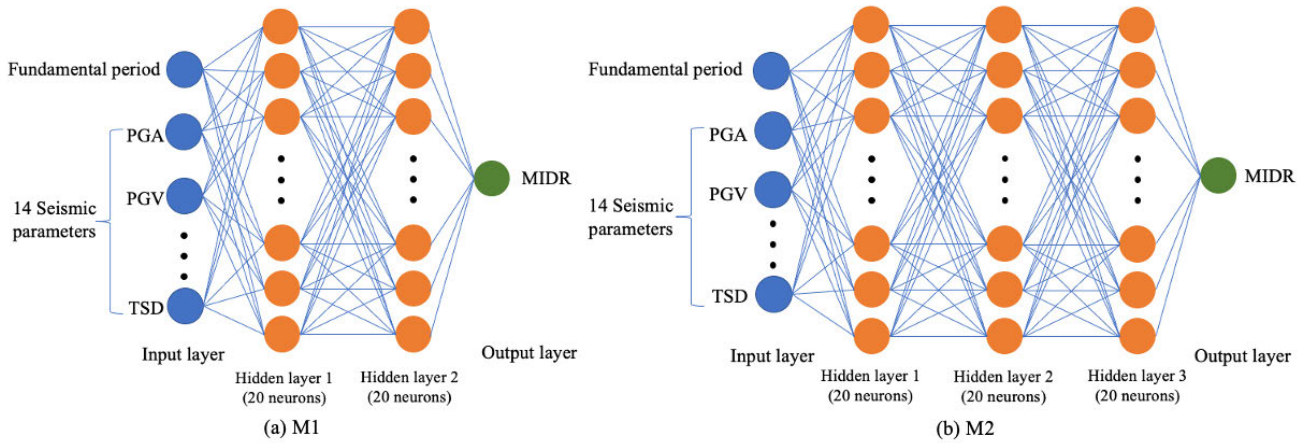
FIGURE 9. The architecture of the first two ANN models. (a) M1 has two hidden layers. (b) M2 has three hidden layers.
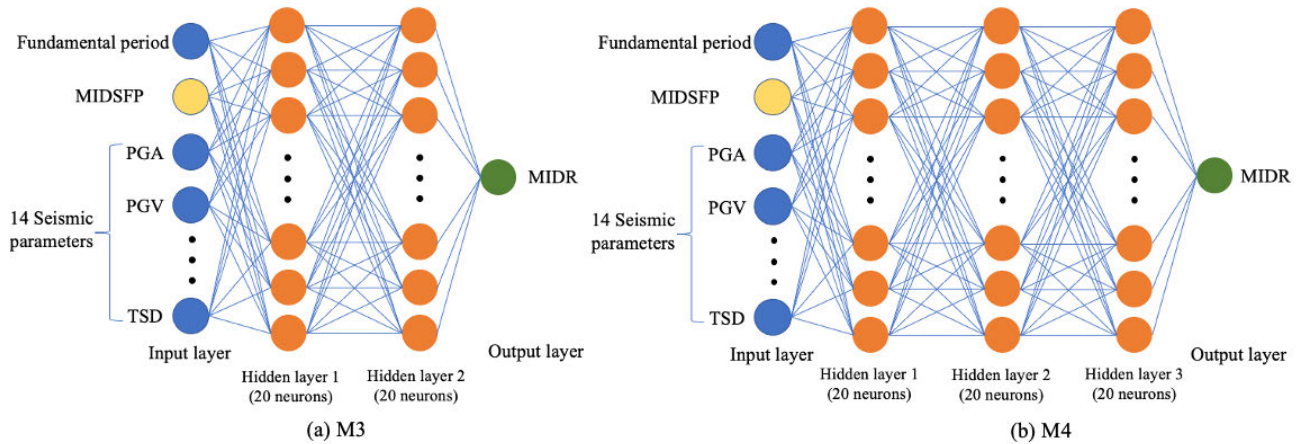

FIGURE 10. The architecture of two ANN models. (a) M3 has two hidden layers. (b) M4 has three hidden layers. (MIDSFP: MIDS of a certain fundamental period).

SVM has many applications in engineering, such as seismic vulnerability assessment[53], [54], micro-seismic events, and blast discrimination [55]. A more detailed description of SVM could be found in the Appendix of the paper [53].

This study also used one SVM model to predict the MIDR. The training set used 14 seismic parameters, fundamental period, MIDSFP as features, and DIDS as the class value. Besides, the radial basis function (RBF) was used as the kernel function. Finally, use the trained model to predict the MIDR.

F. THE FRAMEWORK OF THE PROPOSED METHOD

A detailed framework of the proposed method could be explained as follows, as shown in Figure 11. First, the MIDSs of all seismic events were calculated according to Miranda's model [3], [36]. The MIDSs of 38 earthquakes were calculated from fundamental periods 0.2s to 10s with an interval of 0.2s (491 data). The modal damping ratio ξ_i is 0.05 for each mode, and the MIDS is an average of four cases with $\alpha = 0, 3, 7, 30$. Two kinds of FEMs have different fundamental periods ranges (0.2-3.62s and 1.38-5.82s). Thus, two different parts of the MIDSs (180 data and 288 data out of 491 data) were selected as the input of two DCNNs.

Besides, the THAs of two kinds FEMs were conducted for 38 seismic recordings. The MIDR and the natural frequencies of 30 buildings could be recorded in THA. As a result, the DIDS could be generated by gathering the THA results.

Second, the MIDS and DIDS were fed into the DCNN as the input and output. The network was trained along the direction of decreasing the MSE. During the training process, in the 38 cross-validations, 37 seismic events' results were used as a training set, and the one left was used as a validation set. This process looped 38 times as every seismic event was used as a validation set once. Early stopping was used in the training process to control the training stopping time.

Third, the trained network is used for regression. The MIDS of the left one, which was not used to train the DCNN, was fed into the trained network. The output is regarded as an estimation of the interstory drift spectrum (EIDS). The network was assessed by comparing the EIDS with the THA results.

III. RESULTS AND DISCUSSION

The first section shows that MIDS and DIDS have differences. In the second section, show the DCNN1's results, including the training history and prediction accuracy. In the
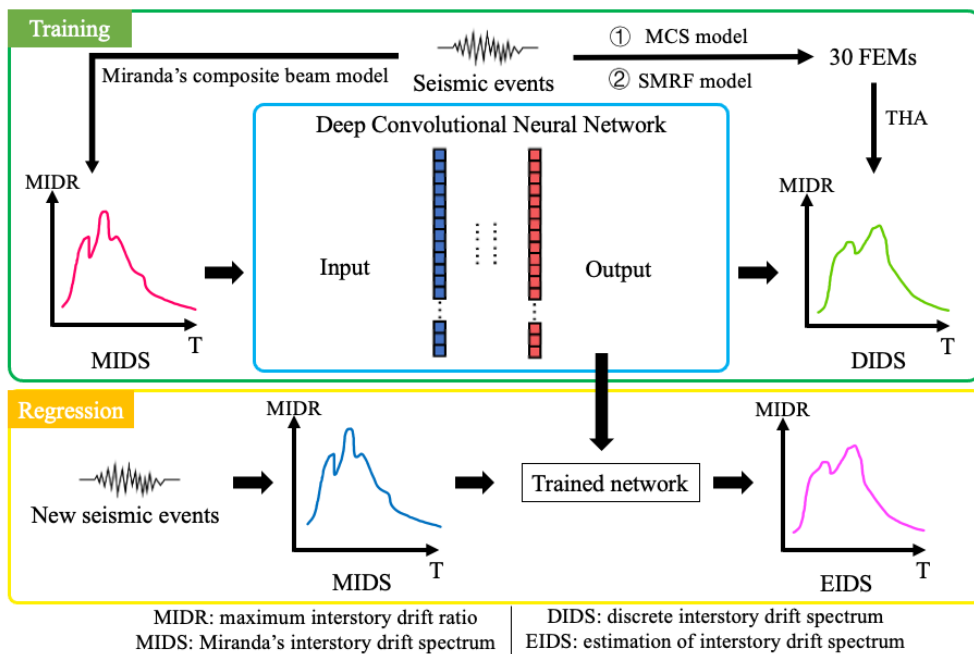
FIGURE 11. The architecture of the proposed method.

third section, use four related ANN models and one SVM model for comparison. Finally, discuss the DCNN2's performance.

A. THE RESULTS OF MIDS AND DIDS

Based on Miranda's theory, the MIDS of 38 seismic recordings were calculated. At the same time, the DIDS could be identified through the MCS models. Take two seismic events as examples (Figure 12). There are differences between the two methods. From Figure 12a, the largest MIDR happens with the natural frequency around 0.5s in seismic event No.1. The DIDS has the same tendency except for periods larger than 1s as the DIDS is higher than MIDS. In Figure 12b, the MIDS is significant at 0.5s and 2.2s in seismic event No.24. However, the DIDS has a different trend as the MIDR is significant within the interval 2s-3.6s.

Miranda had already summarized the different structure types and their corresponding α [3] as follows: shear wall buildings usually have values of α between 0 and 2; buildings with dual structural systems consisting of a combination of moment-resisting frames and shear walls or a combination of moment-resisting frames and braced frames usually have values of α between 1.5 and 6; whereas moment-resisting frame buildings usually have values of α between 5 and 20. The structure type used in the THA is the concrete moment frame, which is close to $\alpha = 7$, according to the above categories. However, MIDS with $\alpha = 7$ is not close to the DIDS in both two cases. The MIDSs of four α (0, 3, 7, 30) all deviate from the MIDS tendency, which implies that other factors will influence the MIDS.

The differences between the THA and the theory are mainly in three aspects: 1. Stiffness ratio α, 2.

The height-wise flexural stiffness and shear stiffness form variation, and 3. The damping ratio of each mode. Manually adjusting these parameters is a blind trial and error process, which will be a time-consuming task to turning parameters involved in the theory, as there will be many different stiffness variation schemes for each α and different damping ratios ξ_i. Therefore, there will be errors to estimate the MIDR of the THA only using the MIDS. Because the number of stiffness variation schemes and damping ratio ξ_i are vast, this study uses a data-driven method to tune the MIDS and give an estimation of the MIDR as the second approximation.

B. THE RESULTS OF THE DCNN1

Take the following steps to estimate the MIDR. First, calculate the MIDS of each seismic event based on Miranda's theory through (1) to (9). The MIDSs of the four α (0, 3, 7, 30) were averaged as a final MIDS. Second, gather the results of the MCS models to obtain the DIDS of each seismic event. Thirdly, train the DCNN1 using the MIDS and DIDS as the input and output. When the MSE of the DCNN1 converged, the network would be well trained. Finally, use the trained DCNN1 to make a regression.

Use two cases (No. 12 and No. 20) for explanations. For seismic event No.12, the MIDSs of left 37 seismic events were used in the training set; the MIDS of No.12 was used as an input of the regression. From the training history in Figure 13, the MSEs of the two cases decrease quickly in the first 100 epochs while converging around 600 epochs. The validation loss decreases along with the training loss. The difference between the training loss and the validation loss is small during the training process, which means the overfitting did not happen.
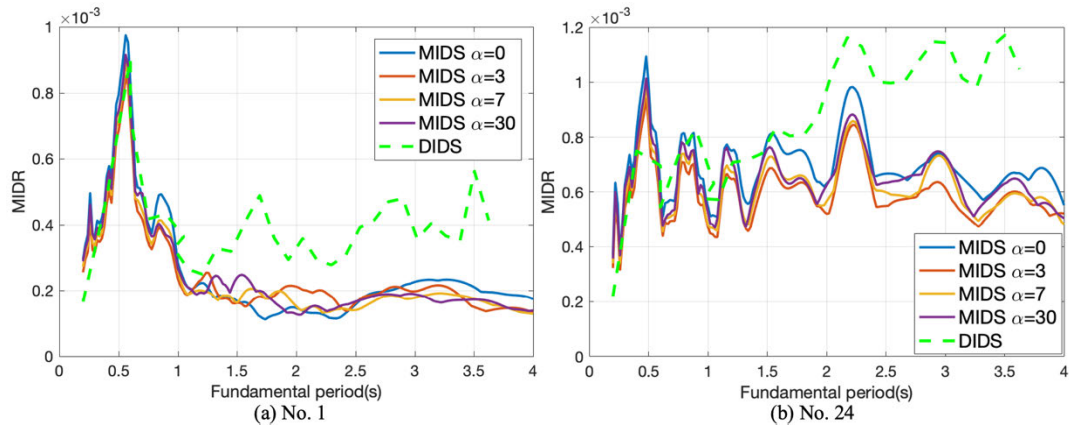
FIGURE 12. The results of MIDS and DIDS. (a) Seismic events No.1. (b) Seismic events No.24.
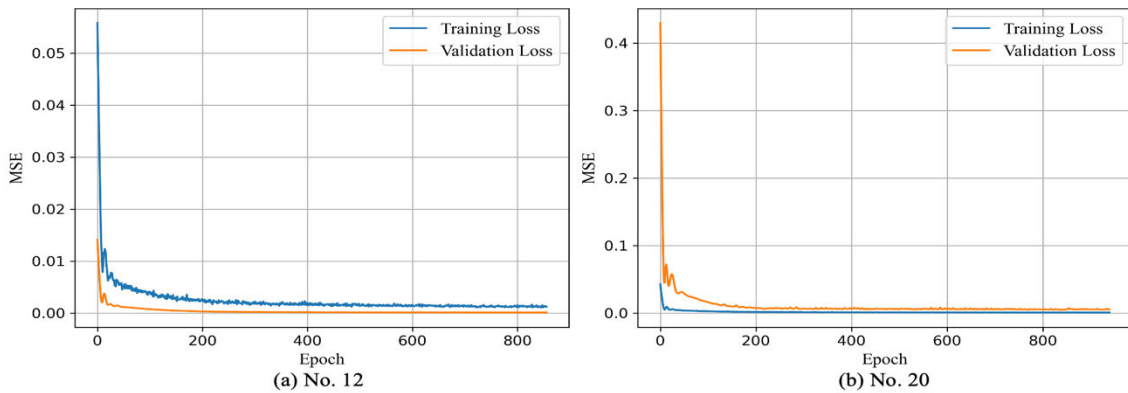

FIGURE 13. Training history of two cases. (a) Seismic event No.12. (b) Seismic event No.20.

The networks' predictions of the two cases are shown in Figure 14. The DCNN1's prediction is much better than MIDS. Although there are still small differences between the DCNN1 and the MCS model, the two lines have a similar trend. The differences between DCNN1 and MCS model are much smaller than the differences between the MIDS and MCS models.

As mentioned above, the MIDS in the validation set has not been used in the training process. Therefore, the DCNN1 learned the nonlinear relationship between the MIDS and the MCS model. The DCNN1 increased the MIDR when the period is greater than 1s. In conclusion, the proposed method could give a reasonable estimation of the MIDR of new seismic events.

Overall, the proposed method includes two estimations. The first estimation utilizes MIDS to estimate the MIDR based on Miranda's theory approximately. The second estimation uses DCNN1 to learn the relationship between the MCS models and MIDS. The results have shown that the proposed method has good performance in prediction.

Firstly, DCNN1 is compared with C1 and C2, as shown in Figure 15a. Clearly, DCNN1 has lower prediction errors. A deeper architecture of the C2 even has an opposite effect on the prediction. Therefore, the architecture, which

has both convolution operations and deconvolution operations (DCNN1), performs better than the architecture with only convolution operations (C1 and C2). Thus, only the DCNN1 is used in the following discussion.

Secondly, compare the six models' prediction (DCNN1, M1, M2, M3, M4, and SVM model) with the MCS models' results. The MSE values between the MCS models and six models are shown in Figure 15b; the vertical coordinates use logarithmic coordinates to show the discrepancy clearly. Figure 15b shows that the DCNN1 has the smallest value in most cases. The small MSE values indicate that the DCNN1's predictions are closest to the MCS models. The MSE of the M3 and the M4 are larger than the DCNN1, which means worse performance. In contrast, M1 and M2 have the worst performance. The MSE differences between the M1 and M2 (or M3 and M4) are almost the same, which means a deeper network of ANN does not significantly improve the prediction accuracy. Besides, MSEs of the SVM model are almost between M1 and M3, which means SVM has greater error than M3 and M4.

To further verify the effectiveness of the DCNN1, the prediction results of the DCNN1, M3, and M4 are compared with MCS models in two scatter plots (Figure 16). In one scatter plot, if the prediction is close to the MCS models, the scatter
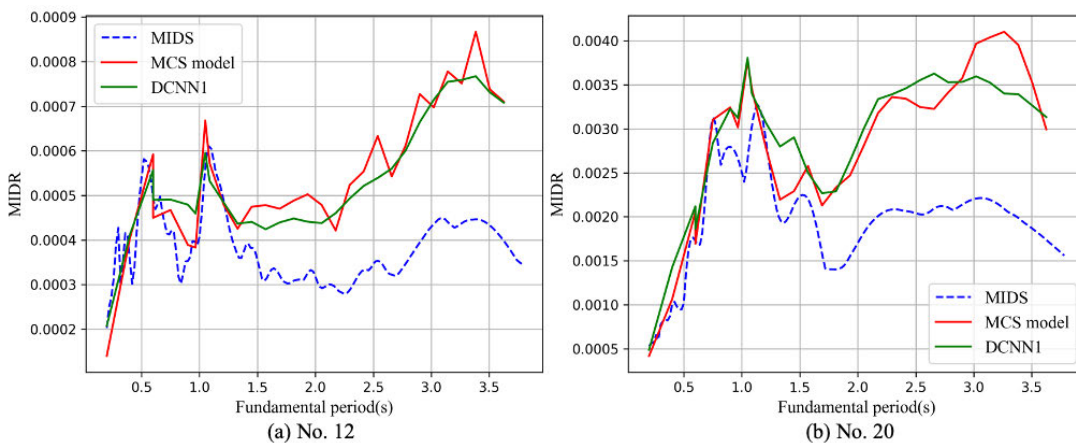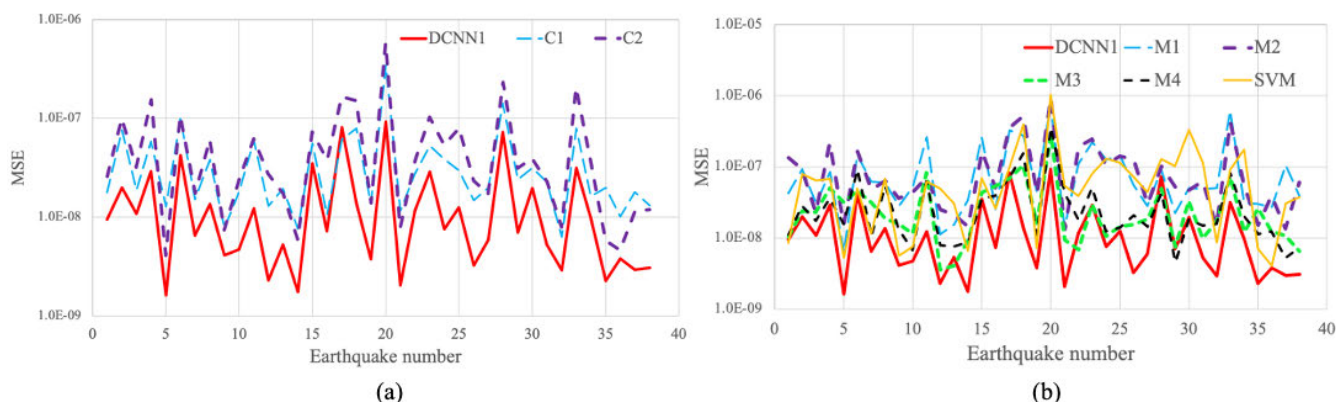
FIGURE 14. The estimation of the DCNN1.

FIGURE 15. MSE comparison of each case. (a) DCNN1 with two CNN models C1 and C2; (b) DCNN1 with five machine learning models.
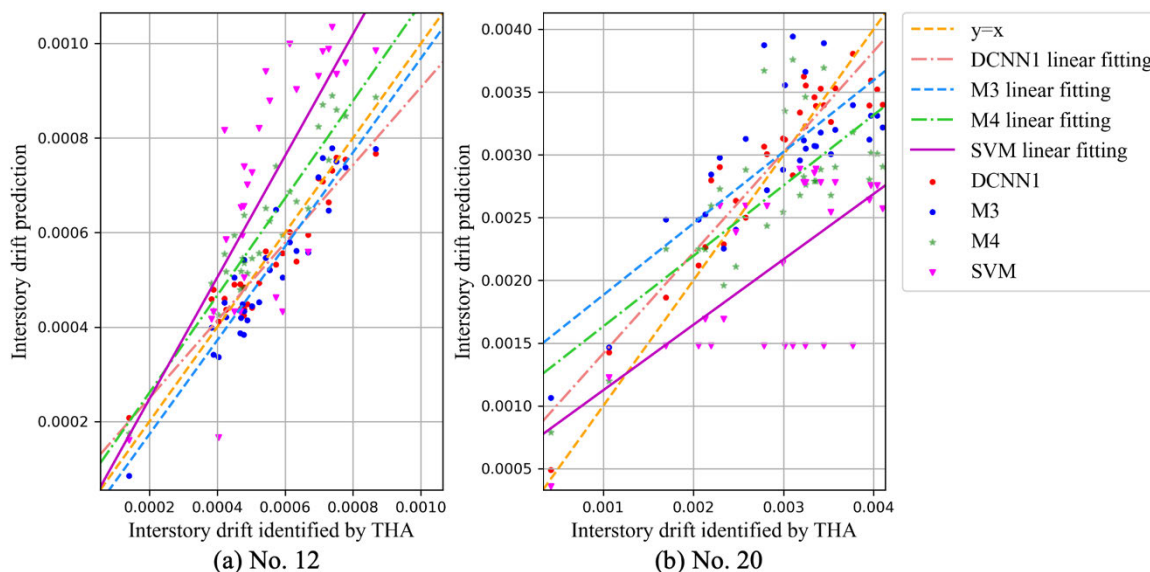

FIGURE 16. Scatter plots of two cases.

points will distribute along the line "y = x." Additionally, linear regression was used to fit the scatter points of each method. Generally, the model is better when the scatter points

locate adjacent to "y = x." Figure 15 shows MSE of case No.12 is close to the average (1.66×10^{-8}); case No.20 has the biggest MSE (9.24×10^{-8}). Take these two cases as
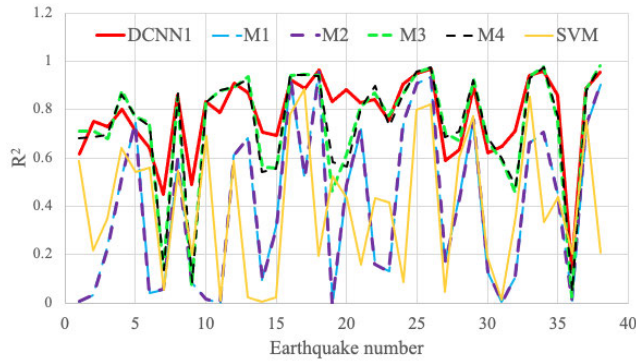
FIGURE 17. R^2 of each model of all cases.

examples to compare the models. The M1 and M2 are not shown in the scatter plot due to the worst MSE.

Clearly, the SVM model has the worst performance in these two cases. The SVM model overestimates the MIDR in No.12. By contrast, the left three models predict the MIDR well. From the linear fitting lines of the three models, the performance descending order is M3, DCNN1, and M4.

Whereas case No.20 is quite different from case No. 12. In case No.20, the scatter points are more dispersive than case No. 12. The prediction points of the SVM model are dispersive in No.20. Thus, the SVM model has the worst performance. In addition, the scatter points of DCNN1 are more concentrated among the three models. Furthermore, the fitted line of DCNN1 is close to "y = x." When the MIDR is less than 0.0025, the M3 and M4 overestimate the MIDR; when the MIDR is greater than 0.0025, the M3 and M4 underestimate the MIDR. To sum up, DCNN1 is the best among the three models in case No.20.

Nevertheless, the above discussions of Figure 16 are qualitative analyses. Quantified indexes are needed to verify the robustness of each model. Index R^2 could illustrate the linear regression quality, as shown in (13):

$$R^2 = 1 - \frac{\sum_i \left(\hat{y}^{(i)} - y^{(i)}\right)^2}{\sum_i \left(\bar{y} - y^{(i)}\right)^2} \qquad (13)$$

where $\hat{y}^{(i)}$ is the predicted MIDR, $y^{(i)}$ is the MIDR of THA, $\bar{y}$ is the MIDR's average. The scatter points have a more linear relationship if the R^2 is big. Until the R^2 reaches 1, all scatter points locate on the fitted line, which means the linear regression will be perfect. Figure 17 shows that the DCNN1 has the largest R^2 than other five models. The average R^2 of the DCNN1, M1, M2, M3, M4 and SVM are 0.78, 0.41, 0.41, 0.74, 0.74, 0.40. This indicates that the DCNN1's scatter points are more concentrated near the fitted line than the four ANN models and the SVM model. Therefore, DCNN1's fitted lines could represent the tendency of the scatter points well.

However, a large R^2 just means the scatter points are more concentrated around the fitted line. It does not mean the fitted line is near "y = x." For example, scatter points could also be concentrated, while they do not concentrate around

"y = x." The slopes and intercepts of five models of 38 cases are calculated (Figure 18) to qualify the difference between "y = x" and all fitted lines. DCNN1's slope values are closer to 1, and DCNN1's intercept values are closer to 0. Therefore, the DCNN1's fitted lines are close to "y = x." Additionally, there are fewer fluctuations of the DCNN1 in both slope and intercepts. By contrast, the four ANN models and the SVM model are not stable in different cases as the slopes and intercepts fluctuate. The standard deviations of the slopes of the DCNN1, M1, M2, M3, M4, and SVM are 0.17, 0.43, 0.47, 0.34, 0.34, and 0.38, respectively; and the standard deviations of intercepts are 1.55×10^{-4}, 5.55×10^{-4}, 5.54×10^{-4}, 3.07×10^{-4}, 2.87×10^{-4}, 2.53×10^{-4}, respectively. The M3 and M4 are more stable than the M1 and M2 mainly due to the feature chosen. In the architecture of M3 and M4, the MIDSFP gives a reasonable initial value of the MIDR. Consequently, the MIDSFP improves the robustness of the ANN model significantly.

Although the M3 and M4 add MIDSFP as an input feature, its robustness is still worse than DCNN1. One reason for this phenomenon is that the 14 seismic parameters could not represent all characteristics of a seismic event. The reason why the MIDS could represent the seismic characteristics is that the MIDS used time history analysis ($D_i(t)$ in (8)) of a single degree of freedom to consider the effects of the ground motions, which will be better than the 14 seismic parameters. Another reason is that the ANN model just used one value of the MIDS, and this value just represents one fundamental period of a structure. For the good performance of the DCNN1, the MIDS, which has a wide range of fundamental periods, could represent the seismic characteristics better than one specific period.

In conclusion, the scatter points of the DCNN1 are concentrated; its fitted lines are closer to "y = x." The above indexes imply that the errors between the THA and the prediction of the DCNN1 are small. Therefore, the DCNN1 has a good ability to predict the MIDR of new seismic events.

C. THE RESULTS OF THE DCNN2

Figure 19 shows the results of the DCNN2. The difference between the MIDS and SMRF is vast due to two damping types (MIDS: the damping ratio of each mode is 0.05; SMRF: Rayleigh damping, the damping ratio of the first mode and third mode are 0.04). Besides, the MIDS and the SMRF have two different fundamental period ranges (0.02s-5.94s and 1.38s-5.82s). The fundamental period range selection is crucial because the MIDS's curve varies along with the range. The similar tendency between the SMRF and DCNN2 means the interstory drift spectrum's characteristics are similar in the two ranges.

The DCNN2 could predict the MIDR's tendency well. From Figure 19, the DCNN2 learns the relationship between the MIDS and SMRF. The DCNN2 increases the MIDR when the MIDS's periods are larger than 2s; it decreases the MIDR in the MIDS's period range 0-2s. As a result, the main tendency of the SMRF has been predicted by the DCNN2.
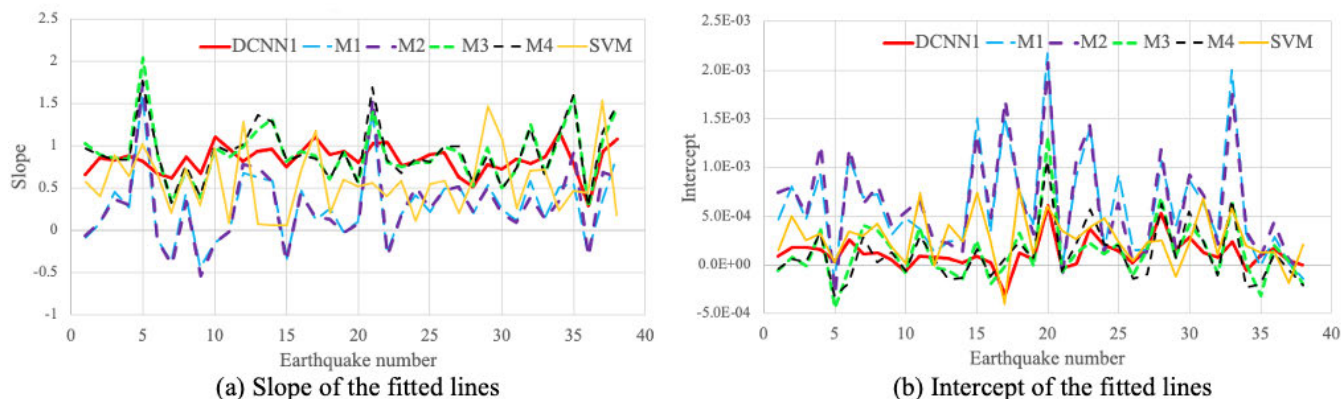
(a) Slope of the fitted lines

(b) Intercept of the fitted lines

FIGURE 18. The slope and the intercept of the fitted lines in the scatter plots.
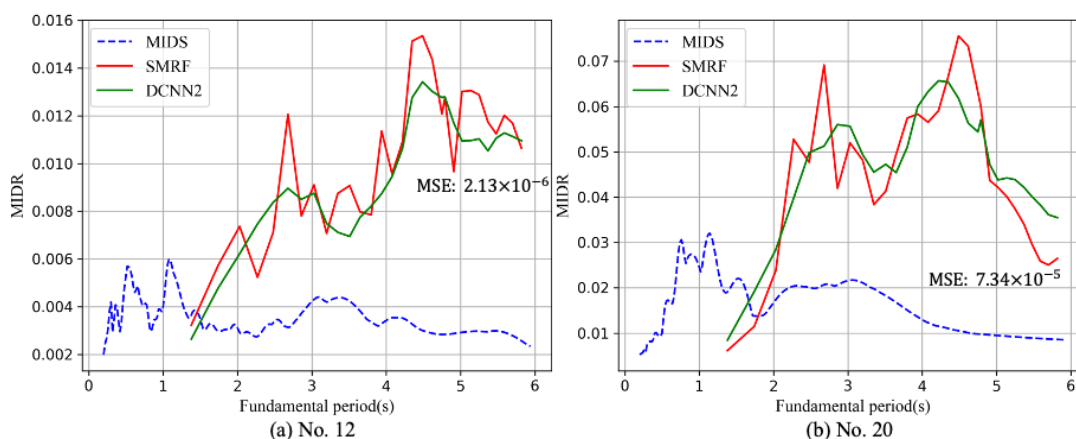

(a) No. 12

(b) No. 20

FIGURE 19. Two cases of the DCNN2.

Nevertheless, the prediction lacks details of the fluctuation. Therefore, the DCNN2 acts as a low-pass filter and removes the MIDS's high-frequency fluctuation.

The drawback of the DCNN2 is the greater MSE than the DCNN1. Figure 19 shows the MSEs of the two cases are 2.13×10^{-6} and 7.34×10^{-5}. Case No.20 has a larger MSE than case No.12, mainly due to a larger amplitude of MIDR (MIDR maximum of No.12: 0.015; No.20: 0.076). The explanations of the drawback are as follows. First, the MCS model's ground motions are scaled one-tenth of its origin, whereas the SMRF models' ground motions are not scaled. Thus, the SMRF models' MIDR is larger than MCS models', leading to larger MSEs. Second, because SMRF models not only have horizontal translation modes but also have rotation modes and vertical translation modes. The SMRF models are more complicated than the composite beam (Figure 2) and the MCS model. Therefore, the DCNN2's predictions deviate from the SMRF models' results.

The results of the DCNN2 indicate that the proposed method could predict the MIDR of more detailed structures. The DCNN2 could predict the tendency of the interstory drift spectrum well.

IV. CONCLUSION

This study's essence is a novel approach using a data-driven method to predict the building's MIDR under seismic effects. The approach includes two approximations: 1. Use Miranda's interstory drift spectrum to give a first approximation of new seismic events; 2. Use a trained DCNN to tune the MIDS given by the first approximation and give a prediction of the interstory drift spectrum as the second approximation. The results turn out that the proposed method's prediction accuracy is good. Based on the investigation above, conclusions could be drawn as follows:

1. In order to estimate the buildings' MIDR under seismic effects, Miranda's interstory drift spectrum was used. However, there are differences between MIDS and the FEM due to the stiffness variation, damping ratio value, and stiffness ratio α. 38 THA were conducted, and each case contains 30 buildings with 30 different story numbers, corresponding to 30 different fundamental periods. The results of 30 THA in one seismic event could identify one DIDS. It has been shown that the differences between DIDS and MIDS exist, and it could not be minimized by only adjusting the stiffness ratio α.

2. The proposed data-driven method uses DCNN to learn the relationship between the MIDS and the MCS models. Both the MIDS and MCS models' results were imported into the DCNN1 for training. In the 38-fold cross-validation, the THA results of 37 seismic events were used as the training set, and the left one was used as the validation set. The trained DCNN1 predicted the left case's MIDR. The results showed the DCNN1 could give a reasonable prediction of the MIDR so that the DCNN1 learned the nonlinear relationship well in the training process. Therefore, the proposed method could predict the MIDR of a new seismic event well.

3. To further show the advantages of the DCNN1, four ANN methods and one SVM model were used for comparison. The first two ANN models (M1 and M2) used one structural parameter and 14 seismic parameters to predict a new seismic event's MIDR. The other two ANN models (M3 and M4) added one MIDS value as a new feature in the input. The SVM model has the same input features as M3 and M4. Four indexes, which are MSE (between the prediction and the DIDS), R^2, slope, and intercept of a fitted line, assessed these methods' prediction performance. The results turn out that MIDS is a vital feature leading to lower MSEs. Thus, M3 and M4 are much better than M1 and M2. The SVM model's performance is between M1 and M3. However, M3 and M4 have low robustness compared with the DCNN1. The DCNN1 has the best performance in prediction with smaller errors and better stability.

4. The results turn out the DCNN2 could predict the tendency of the SMRF models well. The DCNN2 has more layers based on the input data length (288 data). In the DCNN2 design, the selection of the fundamental periods is essential. Due to the SMRF models' complexity, the MSE is larger than the MSE of DCNN1 and MCS models. The DCNN2's performance verifies that the proposed data-driven method could predict the more detailed FEM's MIDR.

This study's future extension is to take more complex building structure models, different structure types, and other field conditions into consideration in the deep learning model. Later, several models should be built on different field conditions. In the future, it is a task to integrate different models into one model, which is competent in various field conditions. Besides, only the elastic demand of MIDR is considered in this study. However, the building structure will experience a nonlinear stage when the ground motion is fierce. Therefore, it is necessary to consider the material nonlinear, whether by a statistical study [5], a FEM [56] or other methods. Additionally, this study just uses MIDR as the engineering parameter. Many other engineering parameters are also crucial under seismic evets like acceleration, residual displacement, fundamental frequency. Proper deep learning networks could be designed to predict these engineering parameters, which should be studied in future work.

REFERENCES

[1] J. P. Moehle, "Strong motion drift estimates for R/C structures," *J. Struct. Eng.*, vol. 110, no. 9, pp. 1988–2001, Sep. 1984.

[2] E. Miranda, "Approximate seismic lateral deformation demands in multi-story buildings," *J. Struct. Eng.*, vol. 125, no. 4, pp. 417–425, Apr. 1999.

[3] E. Miranda and C. J. Reyes, "Approximate lateral drift demands in multi-story buildings with nonuniform stiffness," *J. Struct. Eng.*, vol. 128, no. 7, pp. 840–849, Jul. 2002.

[4] J. Ruiz-García and E. Miranda, "Residual displacement ratios for assessment of existing structures," *Earthq. Eng. Struct. Dyn.*, vol. 35, no. 3, pp. 315–336, 2006.

[5] Y.-Y. Lin and E. Miranda, "Evaluation of equivalent linear methods for estimating target displacements of existing structures," *Eng. Struct.*, vol. 31, no. 12, pp. 3080–3089, Dec. 2009.

[6] A. Alonso-Rodríguez and E. Miranda, "Assessment of building behavior under near-fault pulse-like ground motions through simplified models," *Soil Dyn. Earthq. Eng.*, vol. 79, pp. 47–58, Dec. 2015.

[7] M. Hori, *Introduction to Computational Earthquake Engineering*, 3rd ed. London, U.K.: Imperial College Press, 2011.

[8] P. Latcharote, K. Terada, M. Hori, and F. Imamura, "A prototype seismic loss assessment tool using integrated earthquake simulation," *Int. J. Disaster Risk Reduction*, vol. 31, pp. 1354–1365, Oct. 2018.

[9] A. Sahin, R. Sisman, A. Askan, and M. Hori, "Development of integrated earthquake simulation system for Istanbul," *Earth, Planets Space*, vol. 68, no. 1, pp. 1–21, 2016.

[10] X. Lu, B. Han, M. Hori, C. Xiong, and Z. Xu, "A coarse-grained parallel approach for seismic damage simulations of urban areas based on refined models and GPU/CPU cooperative computing," *Adv. Eng. Softw.*, vol. 70, pp. 90–103, Apr. 2014.

[11] C. Xiong, X. Lu, H. Guan, and Z. Xu, "A nonlinear computational model for regional seismic simulation of tall buildings," *Bull. Earthq. Eng.*, vol. 14, no. 4, pp. 1047–1069, Apr. 2016.

[12] C. Xiong, X. Lu, X. Lin, Z. Xu, and L. Ye, "Parameter determination and damage assessment for THA-based regional seismic damage prediction of multi-story buildings," *J. Earthq. Eng.*, vol. 21, no. 3, pp. 461–485, Apr. 2017.

[13] W. D. Iwan, "Drift spectrum: Measure of demand for earthquake ground motions," *J. Struct. Eng.*, vol. 123, no. 4, pp. 397–404, Apr. 1997.

[14] J. Kim and K. R. Collins, "Closer look at the drift demand spectrum," *J. Struct. Eng.*, vol. 128, no. 7, pp. 942–945, Jul. 2002.

[15] A. K. Chopra and C. Chintanapakdee, "Drift spectrum vs. modal analysis of structural response to near-fault ground motions," *Earthq. Spectra*, vol. 17, no. 2, pp. 221–234, May 2001.

[16] P. Gülkan and S. Akkar, "A simple replacment for the drift spectrum," *Eng. Struct.*, vol. 24, no. 11, pp. 1477–1484, Nov. 2002.

[17] E. Miranda and S. D. Akkar, "Generalized interstory drift spectrum," *J. Struct. Eng.*, vol. 132, no. 6, pp. 840–852, Jun. 2006.

[18] A. H. Shodja and F. R. Rofooei, "Using a lumped mass, nonuniform stiffness beam model to obtain the interstory drift spectra," *J. Struct. Eng.*, vol. 140, no. 5, pp. 1–9, 2014.

[19] A. S. Neam and T. Taghikhany, "Prediction equations for generalized interstory drift spectrum considering near-fault ground motions," *Natural Hazards*, vol. 80, no. 3, pp. 1443–1473, Feb. 2016.

[20] G. Guo, X. Chen, D. Yang, and Y. Liu, "Self-similar interstory drift spectrum and response distribution of flexural-shear beam with nonuniform lateral stiffness," *Bull. Earthq. Eng.*, vol. 17, no. 7, pp. 4115–4139, Jul. 2019.

[21] O. R. de Lautour and P. Omenzetter, "Prediction of seismic-induced structural damage using artificial neural networks," *Eng. Struct.*, vol. 31, no. 2, pp. 600–606, Feb. 2009.

[22] T. K. Šipoš, V. Sigmund, and M. Hadzima-Nyarko, "Earthquake performance of infilled frames using neural networks and experimental database," *Eng. Struct.*, vol. 51, pp. 113–127, Jun. 2013.

[23] K. Morfidis and K. Kostinakis, "Seismic parameters' combinations for the optimum prediction of the damage state of R/C buildings using neural networks," *Adv. Eng. Softw.*, vol. 106, pp. 1–16, Apr. 2017.

[24] K. Morfidis and K. Kostinakis, "Comparative evaluation of MFP and RBF neural networks' ability for instant estimation of R/C buildings' seismic damage level," *Eng. Struct.*, vol. 197, Oct. 2019, Art. no. 109436.

[25] S. Mangalathu, G. Heo, and J.-S. Jeon, "Artificial neural network based multi-dimensional fragility development of skewed concrete bridge classes," *Eng. Struct.*, vol. 162, pp. 166–176, May 2018.

[26] I. Goodfellow, Y. Bengio, and A. Courville, *Deep Learning*. Cambridge, MA, USA: MIT Press, 2016.

[27] S. Li and X. Zhao, "Automatic crack detection and measurement of concrete structure using convolutional encoder-decoder network," *IEEE Access*, vol. 8, pp. 134602–134618, 2020.

[28] Y. Zhang, X. Zhao, and P. Liu, "Multi-point displacement monitoring based on full convolutional neural network and smartphone," *IEEE Access*, vol. 7, pp. 139628–139634, 2019.

[29] C. Modarres, N. Astorga, E. L. Droguett, and V. Meruane, "Convolutional neural networks for automated damage recognition and damage type identification," *Struct. Control Health Monitor.*, vol. 25, no. 10, p. e2230, Oct. 2018.

[30] S. Cofre-Martel, P. Kobrich, E. L. Droguett, and V. Meruane, "Deep convolutional neural network-based structural damage localization and quantification using transmissibility data," *Shock Vib.*, vol. 2019, pp. 1–27, Sep. 2019.

[31] Y. Yu, C. Wang, X. Gu, and J. Li, "A novel deep learning-based method for damage identification of smart building structures," *Struct. Health Monitor.*, vol. 18, no. 1, pp. 143–163, Jan. 2019.

[32] L.-J. Dong, Z. Tang, X.-B. Li, Y.-C. Chen, and J.-C. Xue, "Discrimination of mining microseismic events and blasts using convolutional neural networks and original waveform," *J. Central South Univ.*, vol. 27, no. 10, pp. 3078–3089, Oct. 2020.

[33] G. Fan, J. Li, and H. Hao, "Lost data recovery for structural health monitoring based on convolutional neural networks," *Struct. Control Health Monitor.*, vol. 26, no. 10, pp. 1–21, Oct. 2019.

[34] T. Zhang, S. Biswal, and Y. Wang, "SHMnet: Condition assessment of bolted connection with beyond human-level performance," *Struct. Health Monitor.*, vol. 19, no. 4, pp. 1188–1201, Jul. 2020.

[35] T. Guo, L. Wu, C. Wang, and Z. Xu, "Damage detection in a novel deep-learning framework: A robust method for feature extraction," *Struct. Health Monitor.*, vol. 19, no. 2, pp. 424–442, Mar. 2020.

[36] E. Miranda and S. Taghavi, "Approximate floor acceleration demands in multistory buildings. I: Formulation," *J. Struct. Eng.*, vol. 131, no. 2, pp. 203–211, Feb. 2005.

[37] A. Alonso-Rodríguez and E. Miranda, "Dynamic behavior of buildings with non-uniform stiffness along their height assessed through coupled flexural and shear beams," *Bull. Earthq. Eng.*, vol. 14, no. 12, pp. 3463–3483, Dec. 2016.

[38] J. L. Lin, J. Y. Dai, and K. C. Tsai, "Optimization approach to uniformly distributed peak interstory drifts along building heights," *J. Struct. Eng.*, vol. 145, no. 5, pp. 1–13, 2019.

[39] Pacific Earthquake Engineering Research Center, Berkeley, CA, USA. (2020). *OpenSees*. [Online]. Available: https://opensees.berkeley.edu

[40] *Hazus-MH 2.1: Technical Manual*, Fed. Emerg. Manag. Agency, Washington, DC, USA, 2012, p. 718.

[41] Pacific Earthquake Engineering Research Centre. (2020). *Strong Motion Database*. [Online]. Available: https://peer.berkeley.edu/peer-strong-ground-motion-databases

[42] "Uniform building code," in *Proc. Int. Conf. Building Officials (ICBO)*, vol. 2, Whittier, CA, USA, 1997, p. 2-14.

[43] (2010). *OpenSees Example 6*. Accessed: Nov. 13, 2020. [Online]. Available: https://opensees.berkeley.edu/wiki/index.php/OpenSees_Example_6._generic_2D_Frame,_N-story_N-bay,_Reinforced-Concrete-Section_26_Steel_W-Section

[44] X. Yang, H. Li, Y. Yu, X. Luo, T. Huang, and X. Yang, "Automatic pixel-level crack detection and measurement using fully convolutional network," *Comput.-Aided Civil Infrastruct. Eng.*, vol. 33, no. 12, pp. 1090–1109, Dec. 2018.

[45] Y. Bao, Z. Tang, H. Li, and Y. Zhang, "Computer vision and deep learning–based data anomaly detection method for structural health monitoring," *Struct. Health Monitor.*, vol. 18, no. 2, pp. 401–421, Mar. 2019.

[46] B. Luo, H. Wang, H. Liu, B. Li, and F. Peng, "Early fault detection of machine tools based on deep learning and dynamic identification," *IEEE Trans. Ind. Electron.*, vol. 66, no. 1, pp. 509–518, Jan. 2019.

[47] C. S. N. Pathirage, J. Li, L. Li, H. Hao, W. Liu, and P. Ni, "Structural damage identification based on autoencoder neural networks and deep learning," *Eng. Struct.*, vol. 172, pp. 13–28, Oct. 2018.

[48] A. Nain, S. Paul, and M. Maynard-Reid. (2020). *Keras*. [Online]. Available: https://keras.io

[49] C. Albon, *Machine Learning With Python Cookbook: Practical Solutions From Preprocessing to Deep Learning*. Sebastopol, CA, USA: O'Reilly Media, 2018.

[50] N. D. Lagaros and M. Papadrakakis, "Neural network based prediction schemes of the non-linear seismic response of 3D buildings," *Adv. Eng. Softw.*, vol. 44, no. 1, pp. 92–115, Feb. 2012.

[51] K. Morfidis and K. Kostinakis, "Approaches to the rapid seismic damage prediction of R/C buildings using artificial neural networks," *Eng. Struct.*, vol. 165, pp. 120–141, Jun. 2018.

[52] Seismosoft. (2020). *SeismoSignal*. [Online]. Available: https://seismosoft.com

[53] I. Riedel, P. Guéguen, M. D. Mura, E. Pathier, T. Leduc, and J. Chanussot, "Seismic vulnerability assessment of urban environments in moderate-to-low seismic hazard regions using association rule learning and support vector machine methods," *Natural Hazards*, vol. 76, no. 2, pp. 1111–1141, Mar. 2015.

[54] H. Wu, Z. Cheng, W. Shi, Z. Miao, and C. Xu, "An object-based image analysis for building seismic vulnerability assessment using high-resolution remote sensing imagery," *Natural Hazards*, vol. 71, no. 1, pp. 151–174, Mar. 2014.

[55] H. Wei, W. Shu, L. Dong, Z. Huang, and D. Sun, "A waveform image method for discriminating micro-seismic events and blasts in underground mines," *Sensors*, vol. 20, no. 15, pp. 1–18, 2020.

[56] J. S. Kuang and K. Huang, "Simplified multi-degree-of-freedom model for estimation of seismic response of regular wall-frame structures," *Struct. Des. Tall Special Buildings*, vol. 20, no. 3, pp. 418–432, Apr. 2011.

JINKE LI received the B.S. degree in traffic engineering from Zhengzhou University, China, in 2014. He is currently pursuing the Ph.D. degree with the School of Civil Engineering, Dalian University of Technology, China. His research interests include structural health monitoring and displacement sensor design.

ZHENG HE received the master's degree in building engineering from the Harbin University of Civil Engineering and Architecture, China, in 1996, and the Ph.D. degree in engineering mechanics from the Harbin Institute of Technology, China, in 2000.

From 2003 to 2004, he was an Associate Professor with the School of Civil Engineering, Harbin Institute of Technology. From 2004 to 2010, he was a Professor with the College of Resources and Civil Engineering, Northeastern University. Since 2010, he has been a Professor with the Department of Civil Engineering, Dalian University of Technology. His research interests include modeling and analysis of performance assessment of super high-rise building structures, performance-based seismic design methodology of building structures, parametric modeling, analysis, and design of structures, and precast high-rise concrete structural systems.

Dr. He serves as a reviewer for more than ten English and Chinese journals.
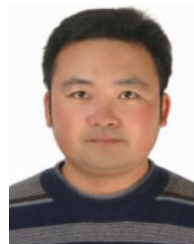
XUEFENG ZHAO received the Ph.D. degree in engineering mechanics from the Harbin Institute of Technology, China.

Since 2007, he has been a Faculty Member with the State Key Laboratory of Coastal and Offshore Engineering, Dalian University of Technology, where he is currently a Professor. He serves as the Director for several projects related to smart sensor network system of structural health monitoring. His research interests include structure health monitoring of infrastructures, structural damage identification, and safety assessment, and application of deep learning in structural health monitoring.

• • •